Journal of Membrane Science 371 (2011) 45–51

Contents lists available at ScienceDirect

Journal of Membrane Science

journal homepage: www.elsevier.com/locate/memsci

Kinetics and mechanism of plasmid DNA penetration through nanopores

Elizabeth Arkhangelsky[a], Yossi Sefi[b], Barak Hajaj[b], Gadi Rothenberg[c], Vitaly Gitis[a,c,*]

[a] Unit of Environmental Engineering, Ben-Gurion University of the Negev, PO Box 653, Beer-Sheva 84105, Israel
[b] Department of Biotechnology Engineering, Ben-Gurion University of the Negev, PO Box 653, Beer-Sheva 84105, Israel
[c] Van't Hoff Institute for Molecular Sciences, University of Amsterdam, Science Park 904, 1098XH Amsterdam, The Netherlands

ARTICLE INFO

Article history:
Received 8 October 2010
Received in revised form 10 January 2011
Accepted 12 January 2011
Available online 19 January 2011

Keywords:
Permeation kinetics
Ultrafiltration
Plasmid elasticity
Viral infection
Polymeric membranes
E. coli

ABSTRACT

DNA transport through membranes is a key step in many biological processes. The phenomenon of DNA penetration through narrow polymer membrane pores was previously observed only under the influence of external electric fields. Recently, it was shown that some types of DNA could penetrate through membrane pores also under hydrodynamic pressure. Here we show that double-stranded plasmid DNA with a 350 nm hydrodynamic diameter penetrates through membrane pores as narrow as 10 nm under pressure, and suggest that the supercoiled plasmids penetrate through these narrow pores by stretching into long hair-shaped flexible strands. We study the kinetics of plasmid penetration and the changes in plasmid elasticity caused by UV irradiation. The results suggest a mechanism based on "snake-like" movement with gradual pore blocking.

1. Introduction

The ever-increasing work on DNA modification and genetic engineering carries a long-term price tag—an increasing danger of environmental contamination. In particular, free plasmid DNA is problematic, as it can lead to genetically new viruses and bacteria [1,2]. Plasmid DNA can infect cells and genomes, multiply, mutate and recombine. Unlike chemical pollutants, which break down and dilute, plasmid DNA is a persistent pollutant. For these reasons it is essential that we understand the mechanism of DNA penetration and transfer through membranes.

Plasmid DNA permeation through membranes is particularly relevant to viral infection mechanisms [3], gene therapy [4,5] and bacterial conjugation [6,7]. Much research was done on this subject, both under well-controlled laboratory conditions [8–12] and using state-of-the-art computer simulations [13,14]. However, the mechanisms by which DNA penetrates through such membranes are still unclear [15,16]. There are conceptual as well as practical difficulties. One problem is that DNA molecules are often much larger than the pores through which they must (and do) penetrate. Another problem is that monitoring this DNA penetration *in vivo* is very complicated.

Many important factors that influence transition of DNA through nanopores have been studied recently. Zydney and coworkers found that higher filtrate flux [17–20], ionic strength [17,21,22] and membrane charge [17] enhance plasmid transition. Morãoa et al. showed that high stirring speeds [20] lowered plasmid transition, due to a suppressed concentration polarization effect. Conversely, the increase in plasmid size had a negative effect [23] or no effect on the plasmid transition [19]. Moreover, the critical flux (the flux needed for significant plasmid transition) increased as pore sizes narrowed [19]. Finally, the plasmid transition depends strongly on the membrane polymer type [23].

Recent calculations showed that the persistence length of linear DNA sequences with different base pairs varies from 47.5 to 74.3 nm [24–26]. Thus, the previously reported results [17–21], [23] can be explained by expanded elasticity of the plasmids that stretch under hydrodynamic pressure. Still, we had a hard time explaining our previous findings [22], namely that double-stranded plasmids had passed through membranes with as little as ~10 nm pore size.

In this paper, we verify that double-stranded circular plasmid DNA penetrates through pores as narrow as 10 nm under hydrodynamic pressure. We study the penetration kinetics by parallel determination of flux and plasmid concentration in the permeate during the run. Dead-end filtration studies are performed using two different plasmids, with hydrodynamic diameters of 320 and 380 nm. The plasmid integrity after the filtration is confirmed through parallel determination of plasmid concentration in competent cells and real-time PCR of triplicate samples. Our results show that DNA plasmids penetrate through pores that are smaller than

* Corresponding author at: Ben Gurion University of the Negev, Biotechnology and Environmental Engineering, PO Box 653, 84105 Beer-Sheva, Israel.
Tel.: +972 86479031.
E-mail address: gitis@bgu.ac.il (V. Gitis).

0376-7388 © 2011 Elsevier B.V. Open access under CC BY-NC-ND license.
doi:10.1016/j.memsci.2011.01.014

the hydrodynamic diameter of supercoiled DNA and even smaller than the calculated persistence length. Subsequently, we irradiated plasmid samples with UV light, increasing the rigidity of the plasmids. As a result, retention of the plasmids increased by as much as 55%. Based on the published studies and our current results, we suggest that the plasmid transition mechanism follows a "snake-like" movement along with gradual blockage of membrane pores with plasmids.

2. Materials and methods

2.1. Bacterial strains and plasmids

Two types of double stranded circular DNA plasmids were used: a 4.5 kilo base pair (kb) pGEMR and a 9.5 kb pHE4-ADR. The pGEMR was constructed by cloning the 1.5 kb fragment into pGEM-T Easy vector (Promega, Madison, WI, USA). The pHE4-ADR (9.5 kb) was constructed by ligation of 6.5 kb fragment into pUHE-24 [27]. The plasmids were grown in *Esherichia coli* and isolated with a NucleoBond PC 500 isolation kit (Macherey-Nagel, Düren, Germany). Average plasmid purity was calculated by absorbance at 260 nm/280 nm and 260 nm/230 nm (1.85 and 1.95, respectively). Transformational experiments were performed with XL-Blue MRF' (Stratagene) or HD5α (Bio-Lab ltd.) competent *E. coli* cells. The recipient cells were thawed on ice for 15 min, mixed with plasmid for an additional 30 min on ice, and heated to 42 °C for 1 min. Incubation was performed for 1 h at 37 °C with 1 ml LB medium. Counting of colony-forming units was performed on LB plates that contained 100 μg/ml ampicillin after 16–18 h of incubation at 37 °C.

2.2. DNA membrane filtration setup

A 150 ml autoclave stirred cell was used (magnetic stirring, 400 rpm) equipped with a back-pressure controller for controlling of transmembrane pressure (TMP). Round, flat membranes of 100 ± 50 nm thickness were supported on a stainless steel support base. Experiments were done at 1.0, 2.0, 3.0, 4.0 and 5.0 bars transmembrane pressure (TMP). Twenty and 30 kDa flat-sheet polyethersulfone (PES) and 10 and 30 nm polycarbonate (PC) membranes (Sterlitech Corporation) were used. The PES membranes were cut into circles with a cross sectional area of 0.025 m^2. The PC membranes were used as received. All plasmids were diluted in deionized water to form the initial suspension of 0.33 μg/ml in 100 ml. To avoid a bias due to concentration polarization, only 30 ml of feed suspension was transferred through membranes at pH 6.0 and a constant temperature of 25 ± 1 °C. The percentage of plasmid rejection was calculated from the plasmid DNA concentrations in the feed and the permeate fractions as

$$\text{Rejection} = \left(1 - \frac{C}{C_0}\right) \times 100\% \quad (1)$$

where C_0 and C are plasmids concentrations in feed and permeate, respectively. The flux through membrane was calculated as

$$J = \frac{\Delta m}{\rho\, \Delta t\, A} \quad (2)$$

where J is the flux ($lm^{-2}\,h^{-1}$), Δm is the permeate weight difference (kg), ρ is the density of permeate ($kg\,l^{-1}$), Δt is the time interval between two Δm measurements (h) and A is the flat sheet membrane area available for filtration (m^2).

2.3. Low-pressure UV irradiation system

A specially designed collimated beam UV apparatus was built to enable us to perform DNA irradiation tests. The apparatus contained a 43-W low-pressure mercury vapor germicidal lamp (Trojan UV, Canada) emitting nearly monochromatic UV radiation at 253.7 nm. The radiation was focused through a circular opening to provide relatively homogenous incident radiation normal to the surface of the plasmid suspension. The lamp and the light path from the lamp to the suspension were enclosed in a wooden box-like enclosure with black-painted interior walls. A stable lamp output was obtained by controlling the airflow around the lamp to keep the operating temperature constant. UV irradiance at 253.7 nm was measured with a radiometer (IL1400; International Light) and UV 254 detector (SEL240) with a filter (NS254). The radiometer had been factory calibrated, traceable to National Institute of Standards and Technology standards, just prior to this study. The suspension of irradiated plasmids was kept in open 100-mm diameter × 15-mm high Petri dish. A suspension of depth 1 cm was magnetically stirred slowly at room temperature (25 °C). A shutter was used to control the exposure time of the suspension to UV light.

2.4. Procedure for DNA characterization

The plasmid DNA solutions were characterized for size and shape by atomic force microscopy (AFM), modifying the preparation protocol of Hansma and Laney [28]. Purified plasmid samples were suspended in 1 mM $NiCl_2$/10 mM Hepes (final DNA concentration 1.0 ppm). 20 μl aliquots were dropped onto freshly cleaved mica, and incubated for 5 min at 20 °C. The samples were rinsed with 1 ml deionized water and dried. AFM measurements were performed at ambient conditions using a Digital Instrument Dimension 3100 instrument mounted on an active anti-vibration table. A 100 μm scanner was used. The 512 × 512 pixel images were taken in tapping mode with a scan size of up to 5 μm at a scan rate of 1 Hz. Dynamic light scattering (DLS) method was used to obtain the plasmid hydrodynamic radius. The measurements were performed with a CGS-3 goniometer equipped with a He–Ne 22 mW 632.8 nm laser. The spectra were collected at angles varying from 30° to 150°. The diffusion coefficient was determined at 30°. The autocorrelation function was calculated by using the ALV/LSE 5003 multiple tau digital correlator. Prior to each measurement, the sample was passed through a 0.8 μm filter to minimise noise.

2.5. Procedure for qualitative analysis using conventional PCR amplification

A 439 bp fragment of pHE4-ADR plasmid (9.5 kb), before and after filtration through PES membrane was amplified using Un4(d) GCATATGATGTAGCGAAACAAGCC and Un4(r) GCGTGACATACCCATTTCCAGGTCC primers, with a Mastercycler gradient thermocycler (Eppendorf, Westbury, N.Y.). Reaction mixtures included a 12.5 μl ReddyMix (PCR Master mix containing 1.5 mM $MgCl_2$ and 0.2 mM concentration of each deoxynucleoside triphosphate), 1 pmol of each of the forward and reverse primers, 1–2 μl of the sample preparation, plus water to bring the total volume to 25 μl. An initial denaturation-hot start of 2 min at 94 °C was followed by 30 cycles of the following incubation pattern: 94 °C for 30 s, 54 °C for 30 s, and 72 °C for 45 s. The PCR products were purified by electrophoresis through a 0.8% agarose gel, stained with ethidium bromide and visualized on a UV transilluminator. The O'GeneRuler™ 1 kb DNA ladder, 250–10,000 bp (Thermo Fisher Scientific) was used.

The ABI prism 7000 Sequence Detection System and SDS Software were used for data analysis. The ABI prism 7000 monitors the fluorescence resonance energy transfer (with a SYBR Green fluorophore) of reaction mixtures, just before the denaturizing step of each amplification cycle and records the cycle number at which fluorescence crosses a specific threshold cycle (Ct) value. The cycle number at which the signal is first detected is correlated with the original concentration of the DNA template, while the starting copy

number of amplicons is inversely proportional to the real time *Ct*. The plasmids, both for detection of membrane rejection ability and as standards were assayed in triplicate. Standard curves were obtained by plotting the *Ct* value of each 10-fold dilution series of plasmids.

2.6. Procedure for quantitative analysis using real-time PCR

The concentration of pHE4-ADR plasmid (9.5 kb) plasmid in feed and permeate fractions were determined by real-time PCR using the following sets of primers: 341F CCTACGGGAG-GCAGCAG and 518R ATTACCGCGGCTGCTGG, Un4(d) GCATATGAT-GTAGCGAAACAAGCC and Un4-r(2) CTCAGCGTACTGAATTTGAGCG, Un4-d(2) GCGTATCTCAAAATGTCCATCTCC and Un4(r) GCGTGA-CATACCCATTTCCAGGTCC. Two sets of opposite primers: pGEM-Fout GACGGCCAGTGAATGTAATACG and pGEM-Rout GTGGC-GATAAGTCGGTCTTACC; pGEM-Fint CGTATTACAATTCATGGCCGTC and pGEM-Rint GGTAAGACACGACTATCGCCAC were used for amplifying the pGEMR plasmid (4.5 kb). Quantification of bacterial DNA was performed in the ABI prism 7000 Sequence Detection System using Absolute QPCR SYBR Green ROX Mix on a 96-well optical plate. The PCR reaction consisted of 10 μl of Absolute QPCR SYBR Green ROX Mix, 150 nM each of forward and reverse primers, and 5.0 μl of each DNA template, in a total volume of 20 μl. Thermal cycling conditions were as follows: 2 min at 50 °C, 15 min at 95 °C, followed by 40 rounds of 15 s at 95 °C and 1 min at 60 °C. To verify that the used primer pair produced only a single specific product, a dissociation protocol was added after thermocycling, to determine dissociation of the PCR products from 60 °C to 95 °C.

The pGEMR (4.5 kb) and pHE4-ADR (9.5 kb) plasmids were used for detecting the membrane rejection ability and as standards for the calibration curves for quantification at six serial dilution points (in 10-fold steps). All runs included a no-template control. Reproducibility of SYBR Green real-time PCR was assessed by running samples independently on different days. The PCR product was verified with ethidium bromide-stained 2% agarose gels. Data analysis was done using the ABI prism 7000 Sequence Detection System and SDS Software. All plasmids were assayed in triplicate. Standard curves were obtained by plotting the *Ct* value of each 10-fold dilution series of plasmids.

2.7. Procedure for transformational experiments

Concentrations of *E. coli* cells before and after the UF membrane were determined using standard culturing methods. 100 μl of *E. coli* XL-Blue MRF' or *E. coli* HD5α cells were plated on LB agar and counted after overnight incubation at 37 °C. The stock solution contained 2×10^8 cfu in ml deionized water and was diluted up to a total volume of 100 ml before filtration. Each experiment was performed at a constant temperature of 25 ± 1 °C and at pH 6.0.

Propagation of T4 bacteriophages was performed by inoculation of the *E. coli* cells at the exponential growth stage (suspension turbidity between 0.2 and 0.3 OD). The culture was incubated overnight at 37 °C. Lysis was performed by adding 300 μl $CHCl_3$. Purification was performed by centrifugation at 6000 rpm for 5 min. The T4 concentration was determined by plaque forming unit (pfu) assay, using the double layer overlay method. After dilution, the initial T4 solution including 1.2×10^6 pfu/ml in deionized water was

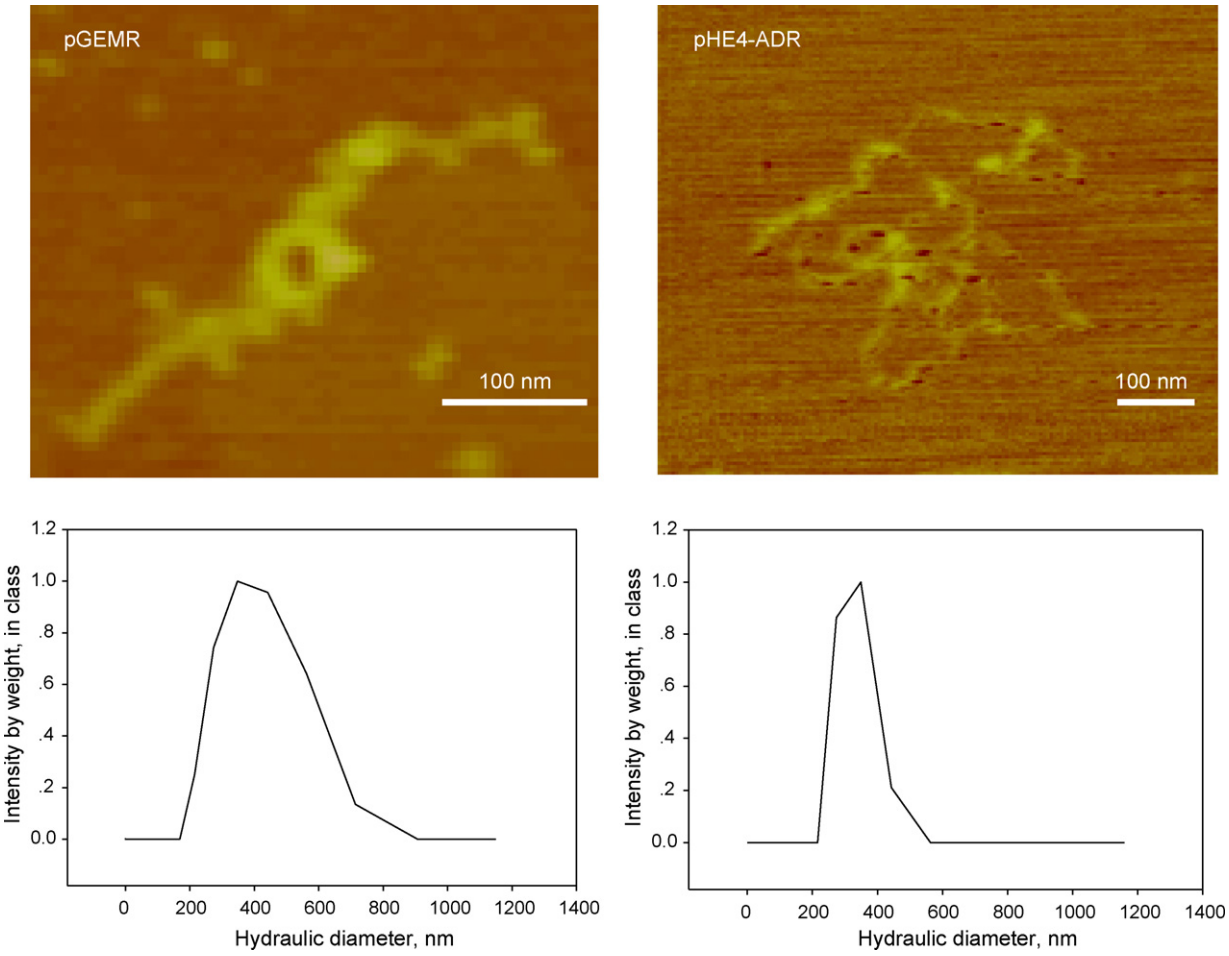

Fig. 1. AFM micrographs (top) and DLS graphs (bottom) of pGEMR and pHE4-ADR. The measurements were performed in deionized water.

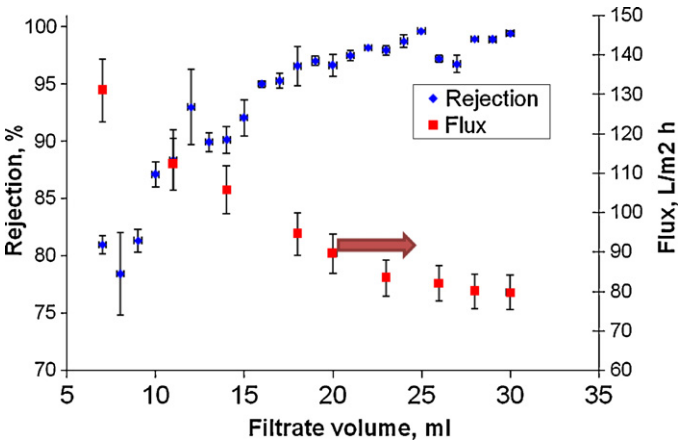

Fig. 2. Observed rejection (blue) and flux (red) values for pGEMR 4.5 kb through 20 kDa PES membrane during the filtration process. *Operating conditions*: TMP 2 bar, *T* 25 °C. (For interpretation of the references to color in this figure legend, the reader is referred to the web version of the article.)

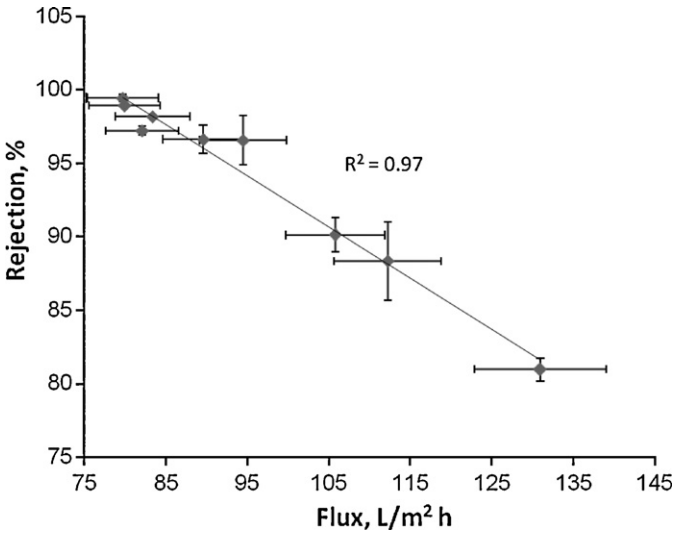

Fig. 3. Observed rejection vs. flux for pGEMR 4.5 kb through 20 kDa PES membranes during the filtration process. *Operating conditions*: TMP 2 bar, *T* 25 °C.

stored at 4 °C. To avoid fouling effects, only 50 ml of feed suspension was transferred through the membranes during the 30 min of experiment.

3. Results and discussion

In a typical experiment, a plasmid solution was placed in a simple dead-end membrane cell. The feed solution was pressured through the membrane that was placed in the bottom of the cell. The permeate samples were collected every 2 ml and analyzed for plasmid concentration.

A series of control experiments was run to verify the membrane pore size, using polyethylene glycol (PEG, 11 experiments with MW from 0.2 to 600 kDa). A 90% rejection (MWCO) was observed between 20 and 25 kDa, in line with the manufacturer's specifications. Filtration of T4 and *E. coli* through uncompromised membranes showed normal log removal values (LRV = 4 and 6, respectively). No change in the values was observed when the membranes' pores were primarily blocked by kaolin. Controlled damaging of the membrane by perforation using a needle resulted in a drastic drop in T4 rejection values from 4 to 0.85 LRV. These results confirm that the membranes were intact and had no pores larger than ~320 nm, which are required for free passage of the supercoiled DNA [29].

The AFM images of pGEMR and pHE4-ADR plasmids showed coiled shapes (Fig. 1) that DNA molecules form in solutions with sufficient ionic strength [30]. The average hydrodynamic diameter

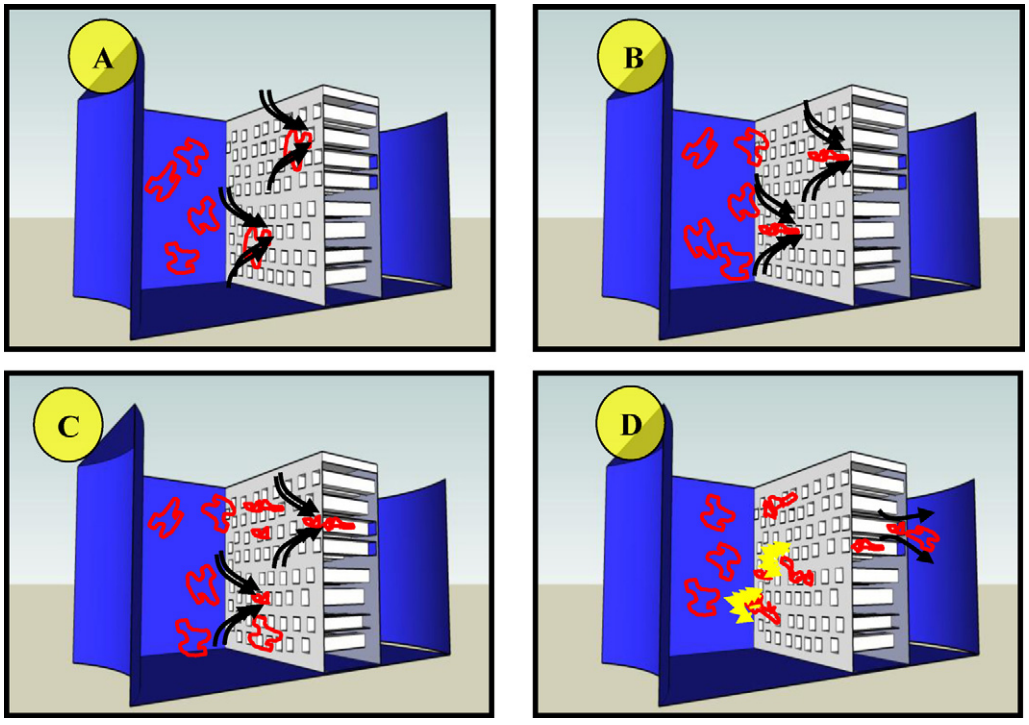

Fig. 4. Possible mechanism of plasmid (in red) penetration through nano-pores (in white). Hydrodynamic pressure (black arrows) is used as a motive force. (For interpretation of the references to color in this figure legend, the reader is referred to the web version of the article.)

of pGEMR is 320 nm and of pHE4-ADR 380 nm. Thus, our results support previous findings [31–37] of higher hydrodynamic sizes for plasmids with higher base pair numbers.

Fig. 2 shows the kinetics of plasmid permeation. Triplicate experiments were run on different days, and triplicate samples were collected at each volume point. The exponential decay in flux from 130 to 80 $lm^{-2}\,h^{-1}$ reflects an increase in rejection from 81% to 99.5%. Fig. 3 shows the correlation between the rejection and the flux. The linear correlation suggests that membrane pores gradually clog with plasmids. This clogging increases the rejection and lowers the flux. The direct relation between flux and transition (in agreement with the results of Zydney and co-workers [18,21]) can be explained as follows: initially, the transportation of plasmids through the pores follows a "snake-like" movement [38,39] due to sufficient hydrodynamic pressure as a moving force. This movement is described by a reptation model and is applicable to transition of polymers through a channel at least twice larger than the polymer size. The maximum plasmid length is 1.45 μm (corresponding to 4.5 kb) and the thickness of the membrane active layer is 10 μm, suggesting that the reptation model applies here. However, large amounts of plasmid remain "plugged" in the pores. This pore blockage leads to a gradual decrease of flux and an increase in DNA retention. The parallel hypothesis of slow plasmid penetration kinetics was ruled out in control experiments performed with 285 ml of solution. The first 30 ml of plasmid-containing solution were followed by flushing with deionized water. No changes in rejection and flux values were observed after first 25 ml.

Fig. 4 shows a possible mechanism for plasmid permeation. Initially, the solution that carries the plasmids moves towards the membrane (Fig. 4A). Close to the pores, some of the plasmids stretch to a form that allows them to enter the pores. Under the hydrodynamic pressure these stretched plasmids enter the membrane (Fig. 4B), and move "snake-like" through it [29,30] (Fig. 4C). They then return to their original supercoiled state after exiting the membrane (Fig. 4D). Eventually, the majority of the pores clog up, plasmid retention rises, and the flux drops by at least 50%.

The above mechanism was supported by a series of additional experiments that verify plasmid integrity, determine the role of plasmid elasticity and relate membrane pore size and plasmid persistence length. The plasmid persistence length as reported recently is between 47.5 and 74.3 nm [24–26] while the membrane's MWCO is between 23 and 25 kDa. A rough estimate is that the membrane main pore size is between 4 and 12 nm. The 4.3 and 6 nm pore size in composite regenerated cellulose (CRC) 30 and 100 kDa membranes was reported [40,41]. This is at least 6–7 times smaller than the plasmid persistence length. The results suggest the presence of

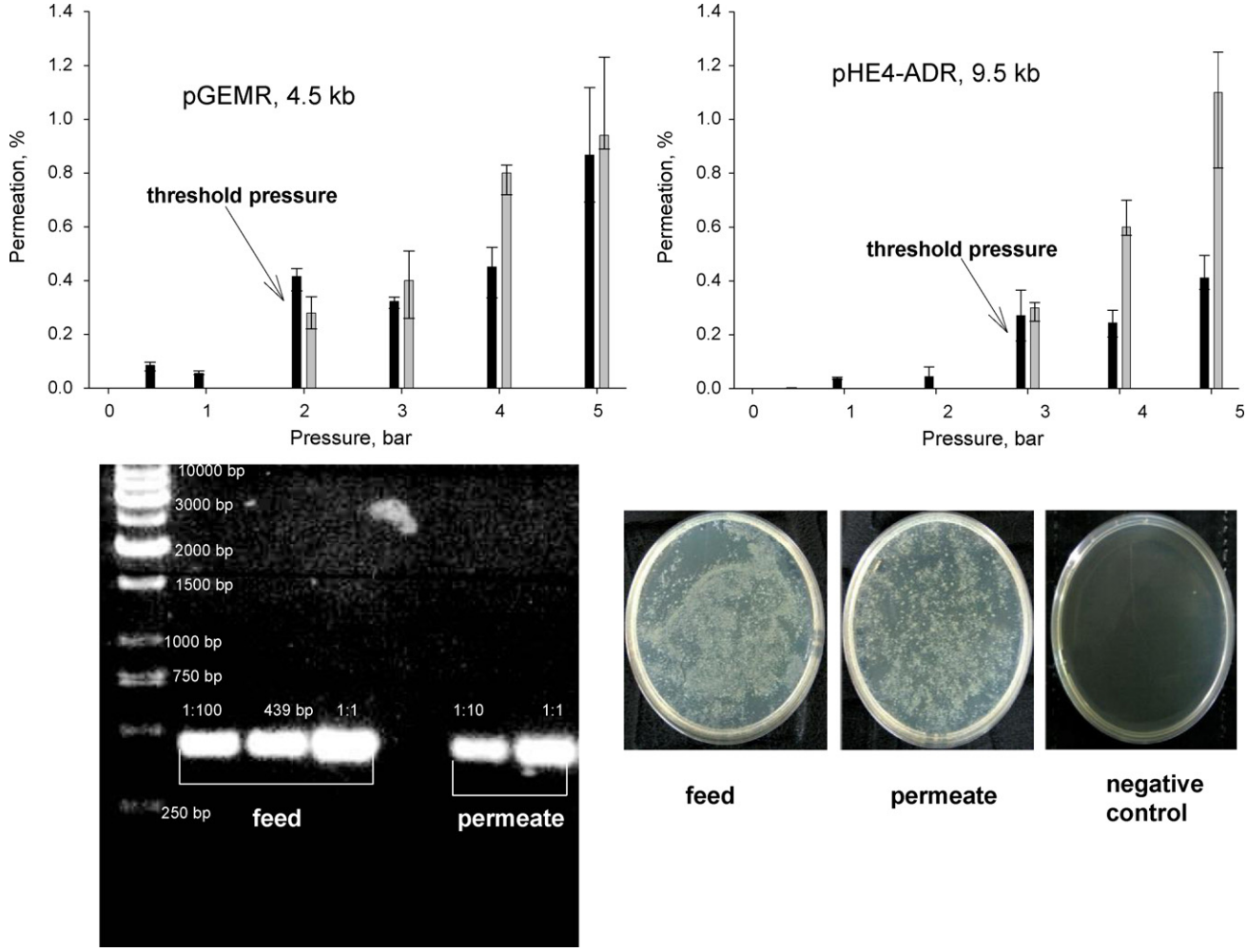

Fig. 5. The % of permeation of pGEMR (top left) and pHE4-ADR (top right) through the membrane at different pressures calculated with real time PCR (black bars), and colony forming units of infected *E. coli* cells (grey bars). All values are averages of triplicate experiments. The image (bottom left) is the gel electrophoresis plates of the PCR amplified 439 bp fragment of pHE4-ADR plasmid (9.5 kb). In each segment, the three bands on the right represent the primary concentration of the plasmid in the feed at different dilutions, while the two bands on the left represent the concentration in the permeate. (Bottom right) *E. coli* DH5-competent cells after pGEMR plasmid transformation: in feed, in permeate, negative control. *Operating conditions*: *T* 25 °C, 30 min, 0.33 ppm plasmid in DI water, PES-20 membrane. The plates are the results of experiments performed at 5 bars TMP.

abnormal pores [42,43] that allow penetration of polymers as large as 50 nm. Although not directly observed, the large pores hypothesis is a widely accepted explanation of frequently reported removal levels of viruses. The number of these pores is limited. As they gradually clog, the retention increases and the flux drops.

The issue of plasmid integrity was assessed in a parallel determination of the plasmid concentration after the membrane cell at different TMPs. The concentrations are presented in Fig. 5 as PCR analysis results (black bars) and corresponding colony numbers of infected *E. coli* cells (grey bars), for TMP values between 1 and 5 bars. Results for pGEMR (top left) and pHE4-ADR (top right) indicate that both plasmids clearly penetrate through the membrane, with values as high as 0.87% for pHE4-ADR at 5 bar overpressure after 30 min. Significantly, both plasmids show similar permeation values, despite the twofold molecular weight difference. The transportation levels depend strongly on the TMP. In each case there is a threshold, above which the penetration begins (3.0 and 2.0 bars for pGEMR and pHE4-ADR, respectively). Blank experiments confirmed that there was no permeation at zero TMP. Transformational experiments showed that both plasmids also retained their infectious characteristics after penetration. Here, the permeate was mixed with *E. coli* cells that were then seeded in Petri dishes and incubated at 37 °C for 16–18 h. The number of colony units correlated with the PCR results (*cf.* the black and the grey bar graphs in Fig. 5). This is one indication that the plasmids retain their original structure. However, it is not a proof, as the *E. coli* itself can in principle repair broken plasmid strands [42]. Additional amplification was performed with two sets of opposite primers (pGEM-Fout and pGEM-Rout; pGEM-Fint and pGEM-Rint). These primers amplified 2.4 kb and 2.1 kb fragments, providing amplification of the entire plasmid and supporting our hypothesis that the plasmid passes whole through the membrane.

We assumed that DNA penetration is enabled by "stretching out" of the plasmid by hydrodynamic forces. Fig. 1 shows that pHE4-ADR has a packed hair-like structure, while pGEMR is completely supercoiled. We suggest that stretching out the packed hair-like structure is easier (*cf.* also the lower percentage of pGEMR in the permeate under identical filtration conditions). The stretching was limited by UV irradiation that causes formation of covalent linkage of two cytosine residues, two thymine residues or one thymine and one cytosine residue. As a result of bonding the plasmid lost its elasticity, forming a rigid structure. Fig. 6 shows the results of UV irradiation at different doses. We see that increased UV doses results in higher retention levels, due to decreased flexibility. The 55% retention obtained at UV dose of 225 J/cm^2 suggests that the transition is due to increased flexibility of the plasmid in its native form. The different plasmid retentions in filtration experiments with PES and PC membranes reflect the difference in membrane pore size and composition.

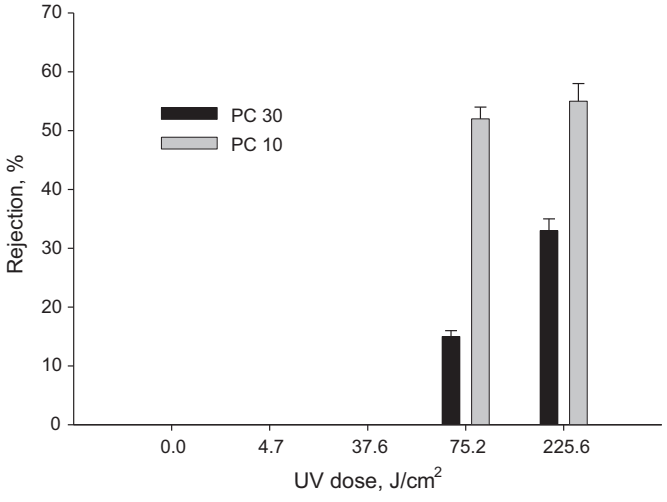

Fig. 6. Rejection of pGEMR as a function of UV dose. *Operating conditions*: TMP 3 bar, *T* 25 °C, PC 10 (grey bars) and PC 30 (black bars).

4. Conclusions

Despite electrostatic repulsion and a significant size difference between plasmid and pore, a circular double stranded DNA molecule can penetrate through synthetic membranes. The penetration is linearly correlated to TMP and is unaffected by plasmid length. Speculating on the possible penetration mechanisms, we suggest that the DNA plasmid is stretched by the pressure and penetrates through the pores as a long hair-shaped semi-flexible string. A critical pressure threshold of 2–3 bars must be reached to stretch out the plasmid. Interestingly, one of the mechanisms for nonenveloped virus transport *in vivo* is transport of naked DNA that might occur due to significant pressure differences on both sides of the membranes. Thus, we believe that the lab results shown here help shed light on the mechanisms of virus transport and cell penetration.

References

[1] W. Doerfler, R. Schubbert, H. Heller, J. Hertz, R. Remus, J. Schroer, C. Kammer, K. Hilger-Eversheim, U. Gerhardt, B. Schmitz, D. Renz, G. Schell, Foreign DNA in mammalian systems, Apmis 106 (1998) 62–68.
[2] M.G. Lorenz, W. Wackernagel, Bacterial gene-transfer by natural genetic-transformation in the environment, Microbiological Reviews 58 (1994) 563–602.
[3] S. Mangenot, M. Hochrein, J. Radler, L. Letellier, Real-time imaging of DNA ejection from single phage particles, Current Biology 15 (2005) 430–435.
[4] E.E. Vaughan, J.V. DeGiulio, D.A. Dean, Intracellular trafficking of plasmids for gene therapy: mechanisms of cytoplasmic movement and nuclear import, Current Gene Therapy 6 (2006) 671–681.
[5] F. Liu, S. Heston, L.M. Shollenberger, B. Sun, M. Mickle, M. Lovell, L. Huang, Mechanism of in vivo DNA transport into cells by electroporation: electrophoresis across the plasma membrane may not be involved, Journal of Gene Medicine 8 (2006) 353–361.
[6] J. Reuther, C. Gekeler, Y. Tiffert, W. Wohlleben, G. Muth, Unique conjugation mechanism in mycelial streptomycetes: a DNA-binding ATPase translocates unprocessed plasmid DNA at the hyphal tip, Molecular Microbiology 61 (2006) 436–446.
[7] M. Llosa, F.X. Gomis-Ruth, M. Coll, F. de la Cruz, Bacterial conjugation: a two-step mechanism for DNA transport, Molecular Microbiology 45 (2002) 1–8.
[8] L. Letellier, P. Boulanger, M. de Frutos, P. Jacquot, Channeling phage DNA through membranes: from in vivo to in vitro, Research in Microbiology 154 (2003) 283–287.
[9] P. Lundberg, U. Langel, A brief introduction to cell-penetrating peptides, Journal of Molecular Recognition 16 (2003) 227–233.
[10] D.J. Zack, M. Stempniak, A.L. Wong, C. Taylor, R.H. Weisbart, Mechanisms of cellular penetration and nuclear localization of an anti-double strand DNA autoantibody, Journal of Immunology 157 (1996) 2082–2088.
[11] M. Ardhammar, B. Norden, P.E. Nielsen, B.G. Malmstrom, P. Wittung-Stafshede, In vitro membrane penetration of modified peptide nucleic acid (PNA), Journal of Biomolecular Structure and Dynamics 17 (1999) 33–40.
[12] R. Brasseur, A. Schanck, B. Delplace, A. De Baetselier, A proposed mechanism underlying the process of Ca-2+-mediated transfer of DNA across biological-membranes, Bioelectrochemistry and Bioenergetics 17 (1987) 111–117.
[13] J.B. Heng, A. Aksimentiev, C. Ho, P. Marks, Y.V. Grinkova, S. Sligar, K. Schulten, G. Timp, The electromechanics of DNA in a synthetic nanopore, Biophysical Journal 90 (2006) 1098–1106.
[14] K.F. Luo, I. Huopaniemi, T. Ala-Nissila, S.C. Ying, Polymer translocation through a nanopore under an applied external field, Journal of Chemical Physics 124 (2006) 114704.
[15] G. Whittaker, Squeezing through pores: how microorganisms get into and out of the nucleus, Trends in Microbiology 6 (1998) 178–179.
[16] I. Chen, P.J. Christie, D. Dubnau, The ins and outs of DNA transfer in bacteria, Science 310 (2005) 1456–1460.
[17] K. Ager, D.R. Latulippe, A.L. Zydney, Plasmid DNA transmission through charged ultrafiltration membranes, Journal of Membrane Science 344 (2009) 123–128.
[18] D.R. Latulippe, K. Ager, A.L. Zydney, Flux-dependent transmission of supercoiled plasmid DNA through ultrafiltration membranes, Journal of Membrane Science 294 (2007) 169–177.
[19] D.R. Latulippe, A.L. Zydney, Elongational flow model for transmission of supercoiled plasmid DNA during membrane ultrafiltration, Journal of Membrane Science 329 (2009) 201–208.

[20] A. Morãoa, J.C. Nunes, F. Sousa, M.T.P. Amorim, I.C. Escobar, J.A. Queiroz, Development of a model for membrane filtration of long and flexible macromolecules: application to predict dextran and linear DNA rejections in ultrafiltration, Journal of Membrane Science 336 (2009) 61–70.
[21] D.R. Latulippe, A.L. Zydney, Salt-induced changes in plasmid DNA transmission through ultrafiltration membranes, Biotechnology and Bioengineering 99 (2008) 390–398.
[22] E. Arkhangelsky, B. Steubing, E. Ben-Dov, A. Kushmaro, V. Gitis, Influence of pH and ionic strength on transmission of plasmid DNA through ultrafiltration membranes, Desalination 227 (2008) 111–119.
[23] S. Kong, J. Aucamp, N.J. Titchener-Hooker, Studies on membrane sterile filtration of plasmid DNA using an automated multiwell technique, Journal of Membrane Science 353 (2010) 144–150.
[24] Y.J. Bomble, D.A. Case, Multiscale modeling of nucleic acids: insights into DNA Flexibility, Biopolymers 89 (2008) 722–731.
[25] C.G. Baumann, V.A. Bloomfield, S.B. Smith, C. Bustamante, M.D. Wang, S.M. Block, Stretching of single collapsed DNA molecules, Biophysical Journal 78 (2000) 1965–1978.
[26] G. Zuccheri, B. Samori, Scanning force microscopy studies on the structure and dynamics of single DNA molecules, Atomic Force Microscopy in Cell Biology 68 (2002) 357–395.
[27] E. Bendov, S. Boussiba, A. Zaritsky, Mosquito larvicidal activity of escherichia-coli with combinations of genes from *Bacillus-Thuringiensis* subsp *Israelensis*, Journal of Bacteriology 177 (1995) 2851–2857.
[28] H.G. Hansma, D.E. Laney, DNA binding to mica correlates with cationic radius: assay by atomic force microscopy, Biophysical Journal 70 (1996) 1933–1939.
[29] The maximum plasmid length was calculated using the conversion factor 10 kb DNA = 104 base pairs = 3.4 micron (see for example Biochemistry, 6th Edition, J.M. Berg, J.L. Tymoczko, L. Stryer, W.H. Freeman, 2007).
[30] T.P. Nguyen, N. Hilal, N.P. Hankins, J.T. Novak, The relationship between cation ions and polysaccharide on the floc formation of synthetic and activated sludge, Desalination 227 (2008) 94–102.
[31] D.M.F. Prazeres, Prediction of diffusion coefficients of plasmids, Biotechnology and Bioengineering 99 (2008) 1040–1044.
[32] D.M. Fishman, G.D. Patterson, Light scattering studies of supercoiled and nicked DNA, Biopolymers 38 (1996) 535–552.
[33] J. Langowski, M. Hammermann, K. Klenin, R. May, K. Toth, Superhelical DNA studied by solution scattering and computer models, Genetica 106 (1999) 49–55.
[34] M. Hammermann, C. Steinmaier, H. Merlitz, U. Kapp, W. Waldeck, G. Chirico, J. Langowski, Salt effects on the structure and internal dynamics of superhelical DNAs studied by light scattering and Brownian dynamics, Biophysical Journal 73 (1997) 2674–2687.
[35] G. Chirico, G. Baldini, Rotational diffusion and internal motions of circular DNA. I. Polarized photon correlation spectroscopy, Journal of Chemical Physics 104 (1996) 6009–6019.
[36] A.M. Campbell, The effects of deoxyribonucleic acid secondary structure on tertiary structure, Biochemical Journal 159 (1976) 615–620.
[37] D.R. Latulippe, A.L. Zydney, Radius of gyration of plasmid DNA isoforms from static light scattering, Biotechnology and Bioengineering 107 (2010) 134–142.
[38] A. Pluen, P.A. Netti, R.K. Jain, D.A. Berk, Diffusion of macromolecules in agarose gels: comparison of linear and globular configurations, Biophysical Journal 77 (1999) 542–552.
[39] H. Shen, Y. Hu, W.M. Saltzman, DNA diffusion in mucus: effect of size, topology of DNAs, and transfection reagents, Biophysical Journal 91 (2006) 639–644.
[40] A. Mehta, A.L. Zydney, Effect of membrane charge on flow and protein transport during ultrafiltration, Biotechnology Progress 22 (2006) 484–492.
[41] A.L. Zydney, A. Xenopoulos, Improving dextran tests for ultrafiltration membranes: effect of device format, Journal of Membrane Science 291 (2007) 180–190.
[42] T. Urase, K. Yamamoto, S. Ohgaki, Effect of pore size distribution of UF membranes on virus rejection in crossflow conditions, Water Science Technology 30 (1994) 199–208.
[43] E. Arkhangelsky, V. Gitis, Effect of transmembrane pressure on rejection of viruses by ultrafiltration membranes, Separation and Purification Technology 62 (2008) 621–630.